Jets, stickiness, and anomalous transport

Xavier Leoncini[1,*] and George M. Zaslavsky[1,2,†]
[1]*Courant Institute of Mathematical Sciences, New York University, 251 Mercer Street, New York, New York 10012*
[2]*Department of Physics, New York University, 2-4 Washington Place, New York, New York 10003*
(Received 20 September 2001; published 4 April 2002)

Dynamical and statistical properties of the vortex and passive particle advection in chaotic flows generated by 4- and 16-point vortices are investigated. General transport properties of these flows are found to be anomalous and exhibit a superdiffusive behavior with typical second moment exponent $\mu \sim 1.75$. The origin of this anomaly is traced to the presence of coherent structures within the flow, the vortex cores, and the region far from where vortices are located. In the vicinity of these regions stickiness is observed and the motion of tracers is quasiballistic. The chaotic nature of the underlying flow dictates the choice for thorough analysis of transport properties. Passive tracer motion is analyzed by measuring the mutual relative evolution of two nearby tracers. Some tracers travel in each other's vicinity for relatively long times. This is related to a hidden order for the tracers, which we call jets. Jets are localized and found in sticky regions. Their structure is analyzed and found to be formed of a nested set of jets within jets. The analysis of the jet trapping time statistics shows a quantitative agreement with the observed transport exponent.

DOI: 10.1103/PhysRevE.65.046216 PACS number(s): 05.45.Ac

I. INTRODUCTION

Transport phenomena can vary from electrons in conducting materials, pollutants in the oceans or atmosphere, or even data across the internet. Typically these phenomena are more often dealing with the transport of macroscopic scalar quantities, such as temperature or density; in other words, systems for which the access to actual microscopic information is beyond reasonable means and in some regards overwhelming if not useless. One of the first major steps towards a proper description of transport arose with the introduction of Fick's and Fourier's laws, which describe, respectively, the evolution of the density and heat current. Assuming further simplifications, both of these laws lead to the well-known heat equation and the related diffusion coefficient. The introduction of the notion of Brownian motion and its associated probabilistic description allowed one to link back this heat equation to the microscopic world, which then is pictured as a collection of random walkers. This may be a rather crude and oversimplified picture of the current problems related to transport, but still today most of this probabilistic spirit remains and in this sense the assumption of some underlying randomness is often made. On the other hand, when considering dynamical systems, the ''microscopic'' quantities are completely or almost completely deterministic and typically evolve with time in a ballistic or accelerated way. As a result there is a strong apparent dichotomy underlying the diffusive or ballistic nature of transport. This dichotomy is directly related to the properties of the underlying dynamics, and in a sense to whether or not the dynamics preserve or lose memory. This diffusive or ballistic nature of transport for a given system is usually inferred by the time evolution of the second moment of its characteristic distribution, namely, $\sim t$ for a diffusive regime and $\sim t^2$ for the ballistic one. Nature is, however, not so reductive and for numerous systems the behavior $\sim t^{\mu}$ with $0<\mu<2$ or even more complicated is observed: transport is so-called anomalous. These anomalous properties result from a subtle interplay of both the diffusive and ballistic behaviors and are linked to Levy-type processes and their generalizations [1–13].

In this paper we address the question of motion of a passive tracer evolving in an unsteady incompressible two-dimensional flow. The underlying problem is related to the transport and mixing in fluids or, more specifically, geophysical flows [14–20]. In order to tackle this problem and especially the anomalous features often observed in geophysical flows, our approach has been gradual and the present work follows from a series of papers [21–25], which consists of successive steps of the investigation of problems of transport in two-dimensional flows from the dynamical point of view. The approach originates from the uncovering of the phenomenon of chaotic advection [26–34], which describes the possible chaotic nature of Lagrangian trajectories in a nonchaotic velocity field and hence reflects a nonintuitive interplay between the Eulerian and Lagrangian perspective. The rise of chaos in these low-dimensional systems allows one to considerably enhance the mixing properties that would otherwise have to rely on molecular diffusion. However, the nonuniformity of the phase space and the presence of islands of regular motion within the stochastic sea has considerable impact on the transport properties of such systems. The phenomenon of stickiness on the boundaries of the islands generates strong ''memory effects'' as a result of which transport becomes anomalous. In this case the rise of anomalous transport can be directly understood by the underlying dynamics, and it makes possible a well-defined probabilistic description [24]. However, typical geophysical flows cannot, in general, be considered as low-dimensional systems, hence one is tempted to consider the method of two-dimensional turbulence (i.e., as high-dimensional system from the dynamical stand point) by introducing some noise term in order to simplify the dynamics of tracers and obtain different properties

*Electronic address: leoncini@cims.nyu.edu
†Electronic address: zaslav@cims.nyu.edu

of this *ad hoc* noise by comparing analytical estimates with experimental or numerical results.

The present approach tackles these problems from another perspective, namely, a relatively simple model is chosen and a thorough analysis of the dynamics of tracers is performed. In other words, instead of introducing noise, we mask our ignorance by simplifying the actual system from the start and take a pure dynamical perspective on the problem. We believe that we may, in this way, shed some light on the kinetics, which actually governs transport, and hence complement the more traditional probabilistic description. To choose a model, we emphasize another peculiarity of two-dimensional turbulent flows, namely, the presence of the inverse energy cascade, which results in the emergence of coherent vortices, dominating the flow dynamics [35–41]. For these systems point vortices have been used with some success to approximate the dynamics of finite-sized vortices [42–44], such as in punctuated Hamiltonian models [41,45,46]. Moreover, point vortices have recently been used to describe the exact unstationary two-dimensional solution of the Navier-Stokes equation [47]; we may thus also envision that the chaotic motion of the vortices shall reproduce to some extent the properties of a more realistic flow. It therefore seems natural to consider a system of point vortices as our paradigm.

In the previously mentioned work, the advection in systems of three- and four-point vortices evolving on the plane has been extensively investigated [21–24]. The three-point-vortex system on the plane has the advantage of being an integrable system and often generates periodic flows (in a co-rotating reference frame) [48–53]. This last property allows the use of Poincaré maps to investigate the phase space of passive tracers whose motion belongs to the class of Hamiltonian systems of 3/2 degree of freedom. A well-defined stochastic sea filled with various islands of regular motion is observed, and among these are special islands also known as ''vortex cores'' surrounding each of the three vortices. Transport in these systems is found to be anomalous, and the exponent characterizing the second moment exhibits a universal value close to 3/2, in agreement with an analysis involving fractional kinetics [23,24]. In this system, the origin of the anomalous properties and its multifractal nature is clearly linked to the existence of islands within the stochastic sea and the phenomenon of stickiness observed around them [23,24]. The motion of N-point vortices on the plane is generically chaotic for $N \geqslant 4$ [54–56]. The periodicity is then lost when considering a system of four vortices or more, but snapshots of the system have revealed that the cores surrounding vortices are robust features [57,58], the actual accessible phase space is in this sense nonuniform and stickiness around these cores has been observed [25]. In order to find out if these properties remain for a large number of vortices, as well as if they may be at the origin of anomalous features of the transport properties of these systems, a thorough analysis is required.

In the following we investigate the advection properties of passive tracers in flows generated by, respectively, 4 and 16 identical vortices. In Sec. II, we recall briefly the dynamics of point vortices and of passive tracers. In Sec. III the dynamics of the system of 16 vortices is investigated and basic properties, such as the time-averaged spatial distribution and minimal intervortex distance, are computed numerically. We observe and describe the formation of the pair and triplet of vortices and obtain statistics of pairing times in a power-law tail, implying finite average of pairing times as well as strong nontrivial memory effects. The measured pairing-time distribution exponent proves to be close to its proposed analytical estimate. In Sec. IV, we consider the motion of a passive tracer in a four-vortex system and develop a new methodology for studying the relative evolution of two nearby ''sticky'' tracers using a notion of chaotic jet [59]. The distribution of trapping times within jets and the associated Lyapunov exponents are computed. The former exhibit a power-law tail. Chaotic jets are located and are directly linked to the sticking behavior of tracers; moreover, their structure is analyzed, which exhibits a nested set of jets within jets. The introduction of a ''geometric'' Lyapunov exponent allows one to characterize each sticky zone independently. The method is then successfully applied to the system of 16 vortices, leading to a possible dynamical mechanism of detecting coherent structures. In Sec. V, we consider transport properties of the 16 vortices as well as those of the tracers in both systems of 4 and 16 vortices. All are found to be anomalous with characteristic exponent $\mu \sim 1.8$, in good agreement with observed trapping times exponent and the kinetic theory discussed in [24].

II. VORTEX AND PASSIVE TRACER DYNAMICS

Systems of point vortices are exact solutions of the two-dimensional Euler equation

$$\frac{\partial \Omega}{\partial t} + [\Omega, \Psi] = 0, \tag{1}$$

$$\Delta \Psi = \Omega, \tag{2}$$

where Ω is the vorticity and Ψ is the stream function. The vortices describe the dynamics of the singular distribution of vorticity

$$\Omega(z,t) = \sum_{\alpha=1}^{N} k_\alpha \delta(z - z_\alpha(t)), \tag{3}$$

where z locates a position in the complex plane, $z_\alpha = x_\alpha + i y_\alpha$ is the complex coordinate of the vortex α, and k_α is its strength, in an ideal incompressible two-dimensional fluid. This system can be described by a stream function acting as a Hamiltonian of a system of N interacting particles (see, for instance, Ref. [60]), referred to as a system of N-point vortices. The system's evolution is

$$k_\alpha \dot{z}_\alpha = -2i \frac{\partial H}{\partial \overline{z}_\alpha}, \quad \dot{\overline{z}}_\alpha = 2i \frac{\partial H}{\partial (k_\alpha z_\alpha)} \quad (\alpha = 1, \ldots, N), \tag{4}$$

where the couple $(k_\alpha z_\alpha, \overline{z}_\alpha)$ are the conjugate variables of the Hamiltonian H. The nature of the interaction depends on the geometry of the domain occupied by fluid. For the case

of an unbounded plane, the resulting complex velocity field $v(z,t)$ at position z and time t is given by the sum of the individual vortex contributions as

$$v(z,t)=\frac{1}{2\pi i}\sum_{\alpha=1}^{N} k_\alpha \frac{1}{\bar{z}-\bar{z}_\alpha(t)}, \tag{5}$$

and the Hamiltonian becomes

$$H=-\frac{1}{2\pi}\sum_{\alpha>\beta} k_\alpha k_\beta \ln|z_\alpha - z_\beta| \equiv -\frac{1}{4\pi}\ln\Lambda. \tag{6}$$

For the motion equations (4), the translational and rotational invariance of the Hamiltonian H provides three other conserved quantities, besides the energy,

$$Q+iP=\sum_{\alpha=1}^{N} k_\alpha z_\alpha, \quad L^2=\sum_{\alpha=1}^{N} k_\alpha |z_\alpha|^2. \tag{7}$$

Among the different integrals of motion, there are three independent first integrals in involution: H, Q^2+P^2, and L^2; consequently, the motion of three vortices on the infinite plane is always integrable and chaos arises when $N \geqslant 4$ [50].

On the other hand, the evolution of a tracer is given by the advection equation

$$\dot{z}=v(z,t), \tag{8}$$

where $z(t)$ represents the position of the tracer at time t and $v(z,t)$ is the velocity field (5). For a point vortex system, the velocity field is given by Eq. (5), and Eq. (8) can be rewritten in a Hamiltonian form as

$$\dot{z}=-2i\frac{\partial\Psi}{\partial\bar{z}}, \quad \dot{\bar{z}}=2i\frac{\partial\Psi}{\partial z}, \tag{9}$$

where the stream function

$$\Psi(z,\bar{z},t)=-\frac{1}{2\pi}\sum_{\alpha=1}^{4} k_\alpha \ln|z-z_\alpha(t)| \tag{10}$$

acts as a Hamiltonian. The stream function depends on time through the vortex coordinates $z_\alpha(t)$, implying a nonautonomous system.

In the following, we focus on systems with $N=4$ and $N=16$ vortices. Due to the chaotic nature of the evolutions, we rely heavily on numerical simulations. The trajectories of the vortices as well as those of the passive tracers are integrated numerically using the fifth-order simplectic scheme described in [61] and which has already been successfully used in [21,23–25].

III. 16-VORTEX SYSTEM FEATURES, PAIRING PROPERTIES, AND SOME STATISTICS

A. Description of the system

We shall start by defining the system of 16 vortices, which we will use to generate the flow advecting passive tracers. As we evolve from the four-vortex system described in [25] to 16 vortices, the phase space is considerably increased and due to the long-range interaction between vortices, the energy does not behave as an extensive variable. However, the constant L^2 defined in Eq. (7) seems to scale as r_{max}^3, where r_{max} is the maximum distance reached between vortices, provided that the origin of our systems corresponds to $Q+iP=0$ and the vortex strengths are all equal and the vortices have approximately a uniform distribution. In order to keep some coherence between the 4-vortex system and the 16-vortex one, we chose to keep the average area occupied by each vortex approximately constant. The switch from 4 to 16 vortices can then be thought of as increasing the domain with nonzero vorticity while keeping the vorticity constant within the patch; in other words, we choose neither to concentrate nor to dilute vorticity while increasing the number of vortices. In light of this, we can write that the area occupied by the vortices is such that $r_{max}^2 \sim N$, and thus $L \sim N^{3/2}$, which leads to $L=64$ for $N=16$ and is our choice for L. The initial condition is chosen randomly within a disk; we choose a configuration such that there are no vortices with close neighborhoods to avoid any possible forced pairing. After that all positions are rescaled to match the condition $L=64$. The resulting simulation shows that the vortices are evolving within a disk of radius ~ 4 (see Fig. 1), which corresponds to $r_{max}^2/N \sim 1$. We recall that for the four-vortex system with $L=4$, we have $r_{max}^2/N \sim 1$ too, and that the expression $L \sim N^{3/2}$ is not correct for only four vortices.

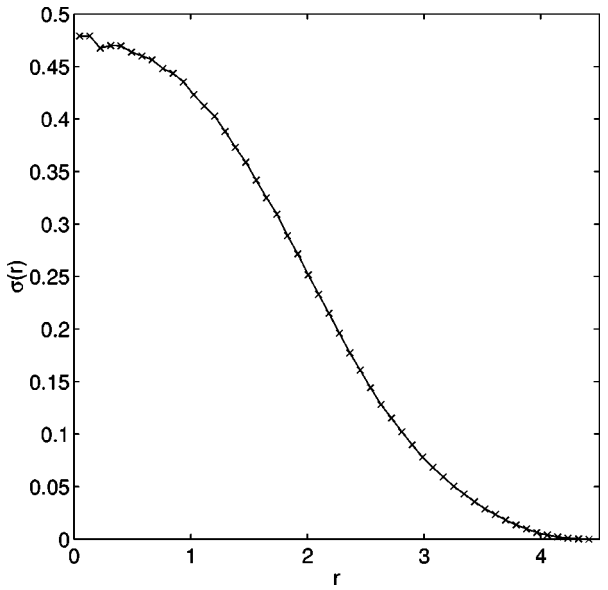

FIG. 1. Spatial density distribution of the vortices obtained with one trajectory computed up to $t=10^5$ (corresponding to 1.6×10^6 data points). Due to vortex nondifferentiation (permutation symmetry) and the rotation invariance, the density depends only on r, i.e., on the distance from the center of vorticity, and it is identical for each individual vortex with the same r. We notice a bell-shaped distribution, which is reminiscent of the Lamb-Oseen vortex.

We can see in Fig. 1 that the time-averaged spatial distribution of the point vortices is not uniform; it has a bell shape that reminds us of an extended vortex, such as the Lamb-

Oseen one. The stationary distribution illustrated in Fig. 1 is a time averaged and, in general, it cannot be associated with an extended stationary solution of the Euler equation (1). We shall not go into further detail, but this nonuniformity by concentrating vortices in the center is likely to lead to differences between the 4- and 16-vortex systems, especially regarding the minimum intervortex distance and the resulting core size, which, as will be seen later, are both much smaller in the 16-vortex system than in the 4-vortex one.

We now move on to vortex pairing and pairing-time distributions.

B. Minimum distance between vortices, vortex pairing, and triplets

It has been found in Ref. [25] for a 4-vortex system that the pairing of vortices dramatically influences the trapping of tracers at the periphery of the vortex cores. Namely, the pairing allows the sticky region around the cores to exchange trapped tracers, while ''opening the door'' for new tracers to be trapped or for some to escape. Since the same behavior should occur with 16 vortices, we decided to investigate the pairing behavior of the considered 16-vortex system. For this purpose we carried out a simulation up to $t=10^5$ and checked the behavior of intervortex distances versus time. The results indicate that long time vortex pairing exists and one vortex pairing that lasts $\Delta t \sim 10^4$ is illustrated in Fig. 2. We also note that during the pairing a triplet (a system of three bound vortices) is formed for about $\Delta t \sim 500$. The phenomenon of formations of triplets and pair of vortices concentrates vorticity in small regions of the plane (see Fig. 3) and in some sense is reminiscent of the inverse energy cascade observed in two-dimensional turbulence. Since no quadruples are observed, we recall that both systems of two and three vortices are integrable, and we may hence wonder whether the observation of triplets and pairs is just pure coincidence or that the long memory effects associated with stickiness are intimately linked to this type of behavior. Namely, for passive tracers in the three-vortex systems, the phenomenon of stickiness is associated with tracers that stay a ''long time'' in the vicinity of an island and mimic the regular trajectory of tracers trapped within the island. This notion was somewhat extended in [25], where the pairing behavior in the four-vortex system was described as a sticking phenomenon to an object of lesser dimension than the whole phase space. However, we speak about the pairing in the four-vortex system as a reduction to an integrable three-vortex system. It is, therefore, tempting to generalize this behavior as a sticking phenomenon to an object of lesser dimension than the actual phase space, but with some constraints. The subspace is reached by generating subsystems whose integrability is a good approximation for a fairly long time. In this light, stickiness would impose some conditions on the actual structure of potential clusters of vortices, for instance, quadruples will be possible to encounter only if two out of the four vortices are involved in a pairing on a smaller scale, giving rise to a triplet on a larger scale. However, we have neither confirmed nor ruled out this scenario with the system of 16 vortices, and hence we shall keep for now the simpler generalized notion of stickiness defined in [25,62,66]. In any case, both the triplet and pairing events described in Fig. 2 correspond to a sticking behavior, as the system remains a long time on a given subset of the phase space. For comparison we mention that a typical time of an eddy turnover used in [16] corresponds to a time of order $\Delta t \sim 1-5$.

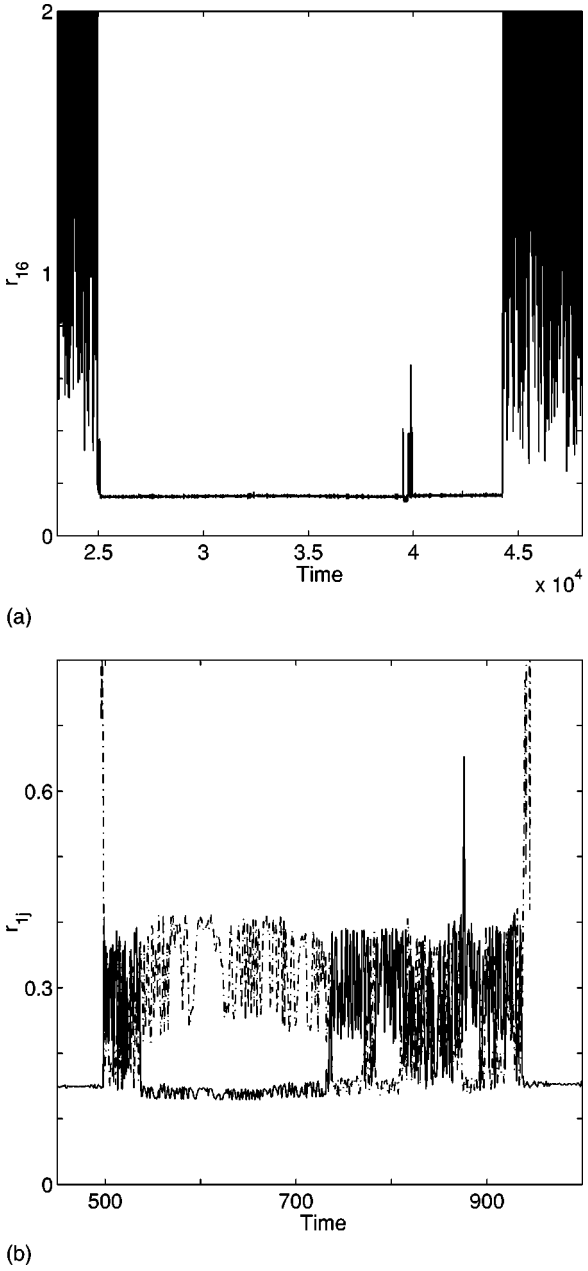

FIG. 2. Observation of a very long pairing of two vortices: (a) $\Delta t \approx 2\times 10^4$. We notice a bump in the pairing around $t=4\times 10^4$. Analysis of this bump reveals the formation of a triplet of vortices (b), which lasts about $\Delta t \approx 450$, which is still very large compared to typical time scales. In (a) the relative distance between vortices 1 and 6 is plotted versus time, while in (b) we added also the relative distance between vortices 1 and 16 (dashed line) for the time length of the observed bump.

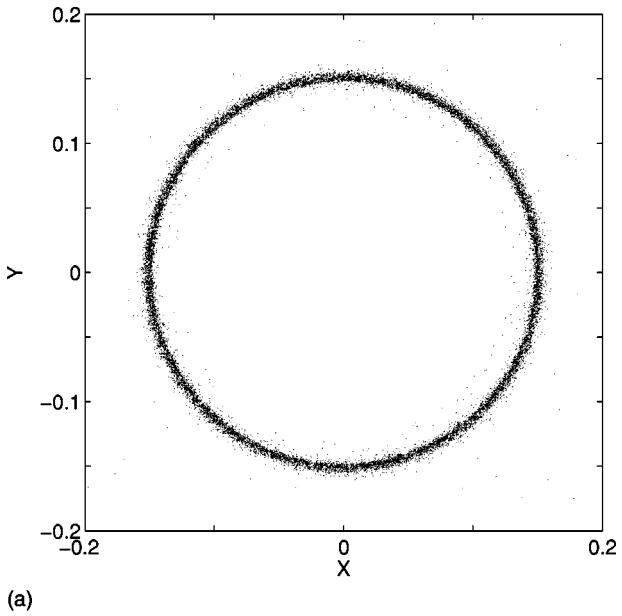

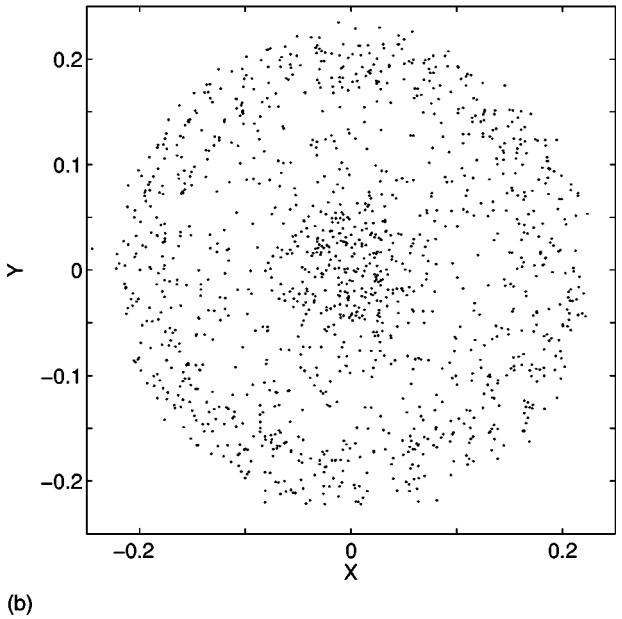

FIG. 3. In this figure the relative positions of the vortices involved in the pairing, corresponding to Fig. 2, are plotted. (a) shows the position of vortex 6 relative to vortex 1 versus time. (b) shows the positions of vortices 1, 6, and 16 relative to their center of vorticity. In both cases we notice that the space occupied by the system has a typical radius of around 0.2, which is to be compared to an average area occupied by each vortex of ~ 1.

Finally, by detecting the pairing of vortices we were, at the same time, able to measure the minimum distance between vortices. It was suggested in [57] that the minimum distance can be a pretty good indicator of the double size of the vortex cores surrounding the vortices [24,25]. We found out that $\min(r_{ij}) \approx 0.13$, which implies that the core radius estimate r, given by a half of the minimum of the intervortex distance, should be of the order $r \sim 0.065$.

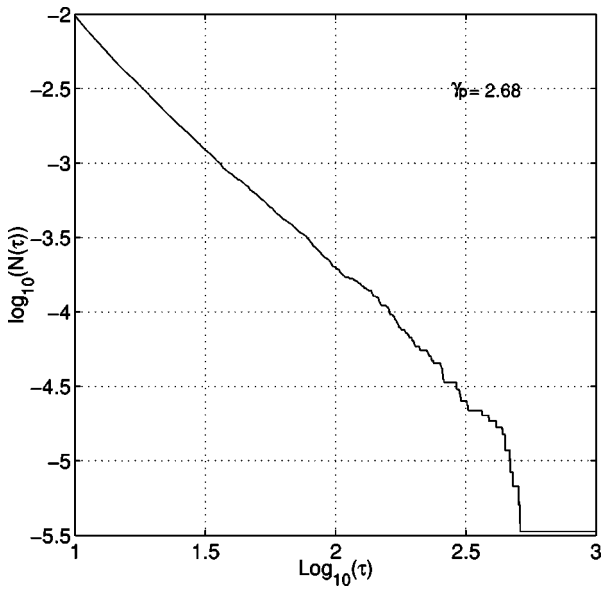

FIG. 4. Distribution of integrated pairing times [see definition (11)] for the system of 16 vortices.

C. Paring-time statistics

In the previously mentioned works [23,24], it has been shown that the stickiness, providing long coherent motion, leads to anomalous transport properties and distributions with power-law tails. We will show how the vortex pairing is related to the stickiness phenomenon and how it influences the motion of passive tracers. Following the methodology and the results presented for four vortices in [25], we consider statistical data on pairing times for the 16-vortex system, using the previously run simulation of vortex motion up to time $t = 10^5$. The detection of pairing events is obtained with the same technique directly inspired by Fig. 2: a pairing occurs if for a given length of time two vortices stay close together. The results obtained for the four-vortex system were independent of the arbitrary cutoffs chosen to characterize a pairing event, hence we chose the arbitrary time length to be $\delta t = 5$ (this value does not affect the behavior of large pairing time), and the distance from one vortex to another is such that $r_{ij} = |z_i - z_j| \leqslant 1$. To gather the statistics, we proceed as was done in [25] and compute the the integrated probability $N(\tau)$ of pairings that last longer than a time τ

$$N(\tau) = N(T > \tau) \sim \int_{\tau}^{\infty} \rho(T)\, dT, \tag{11}$$

where $\rho(T)dT$ is the probability density that an event will last a time T. The results are shown in Fig. 4. The analysis of the distribution tail gives a power-law decay of $N(\tau) \sim \tau^{-\gamma_p + 1}$ with the pairing exponent $\gamma_p \sim 2.68 \pm 0.1$ that confirms the non-negligible occurrence of long-lasting pairings.

The behavior of the probability density of pairing $\rho(\tau)$ lasting a time τ is obtained from Eq. (11) as

$$\rho(\tau) \sim \frac{dN}{d\tau} \sim \frac{1}{t^{\gamma_p}}. \tag{12}$$

This behavior provides a finite mean pairing time, but the second moment is infinite if the value of γ_p can be extrapolated. As suggested in the following section, pairing leads to one of the many forms of stickiness, hence the pairing times are to link to the trapping time within a sticky domain of phase space and parameters.

In the following section, we provide an estimate of γ_p.

D. Pairing exponent

The main idea used to estimate the value of the paring exponent γ_p follows the results presented in Refs. [67] and [24]. The idea revolves around the presence of an island of stability leading to ballistic or accelerator modes within the island. These islands appear in the stochastic sea as a result of a parabolic bifurcation [63] and correspond to the so-called tangled islands [64,65]. This is fairly general and it is reasonable to link the sticky phenomenon of vortex pairing to the rise of an island in the stochastic sea, i.e., the formation of a virtual potential well for the dynamics of a pair of vortices. Another way to validate this point of view comes from the pair perspective. While the pair exists, an integrable system is formed which is perturbed by the flow generated by other vortices. To deal with the problem we use the general form of effective Hamiltonian proposed in [63] (see also [67] and [66]),

$$H_{eff} = b(\Delta P)^2 - a\Delta Q - V_3(\Delta Q), \tag{13}$$

where ΔP and ΔQ are, respectively, the generalized momentum and the generalized coordinate of the pair of vortices, the interaction potential V_3 is a third-order polynomial, and a, b are constants. The higher-order terms in ΔQ can be neglected for the effective Hamiltonian.

Let us assume that the pairing corresponds to the occurrence of an island in the stochastic sea and that effective regular trajectories of the pair can be described by H_{eff} given in Eq. (13). This island has an elliptic point $\xi_e = (P_e, Q_e)$. Since the island has a finite size, a typical trajectory $\xi = (P,Q)$, located within the island corresponds to periodic or quasiperiodic dynamics and can be characterized by its relative coordinates $(\Delta Q, \Delta P) = \xi - \xi_e$. When the boundary of the island is reached, the values of the generalized coordinates $\xi^* = (P^*(t), Q^*(t))$ are such that the trajectory can access the whole stochastic sea, but cannot enter the island (the generalized phase space is two dimensional).

The following steps are fairly formal (see also [66] and [24]). Let us consider a trajectory which is close to the island's edge, which we monitor by the coordinates $(\delta P, \delta Q) = \xi - \xi^*$. A small perturbation is then likely to allow the trajectory to ''escape'' from the island vicinity and consequently to destroy the vortex pair. The phase volume of the escaping trajectory is

$$\delta\Gamma = \delta P\, \delta Q, \tag{14}$$

where δP and δQ are the values of the escaping trajectory. Since the trajectory is close to the island's edge (inflexion point), we can estimate from Eq. (13)

$$\delta P \sim \delta Q^{3/2}, \tag{15}$$

where we have assumed $V_3(Q) \sim Q^3$. Using this last expression (15), we obtain for Eq. (14)

$$\delta\Gamma = \delta Q^{3/2} \delta Q \sim \delta Q^{5/2}. \tag{16}$$

Due to the periodic or quasiperiodic nature of the trajectories within the island, any sticking trajectory (in its neighborhood) experiences a ballistic-type behavior, which translates into $\delta Q \sim t$, i.e.,

$$\delta\Gamma \sim t^{5/2}. \tag{17}$$

The probability density of escaping the island vicinity after being in its neighborhood for a time t (i.e., time length of the pairing) within an interval dt is then

$$\rho(t) \propto 1/\delta\Gamma(t) \sim t^{-5/2}. \tag{18}$$

This result gives us directly the estimate of the exponent $\gamma_p \approx 5/2$, which is very close to the observed value 2.7 ± 0.1.

This estimate is not rigorous and is based on phenomenological grounds; however we believe it provides good insight into the origin of different characteristic exponents of trapping time distributions. We now remind the reader that for the 4-vortex system the value observed in [25] for a characteristic exponent was $\gamma_p \approx 7/2$. This value was explained in a very similar way to that just developed but one more generalized spatial coordinate was introduced. A 4-vortex system is nongeneric. Indeed, as a pair is formed, the whole system becomes a quasi-three-vortex system, the pair acting as one vortex with increased strength, hence the remaining system is itself integrable. In light of this, when switching to the idealized generalized variables (P,Q), we should consider more degrees of freedom to describe the pair of vortices, namely,

$$H_{eff} = c_1(\Delta P_1)^2 + c_2(\Delta P_2)^2 + V_3(\Delta Q_1, \Delta Q_2). \tag{19}$$

The Hamiltonian (19) is, in general, nonintegral, and the appearance of an island of stability adds an additional constraint or integral of motion to the system governed by Eq. (19). Taking this constraint into account, the Hamiltonian (19) can be transformed into

$$H_{eff} = c(\Delta P)^2 + V_3(\Delta Q_1, \Delta Q_2), \tag{20}$$

where ΔP is a new (collective) momentum. The corresponding phase volume of the escaping trajectories gives, in analogy to Eq. (14),

$$\delta\Gamma = \delta P\, \delta Q_1\, \delta Q_2 \sim \delta Q^{5/2} \quad (Q \sim \delta Q_{1,2}). \tag{21}$$

This leads to the estimate of $\gamma_p \approx 7/2$, in contrast to Eq. (18) with $\gamma_p \approx 5/2$. Note that the extra spatial generalized coordinate introduced in [25] can also be thought of as a consequence of having two different coexisting quasi-integrable subsystems described by different actions, but linked as they cannot ''live'' without one another.

We now have a sufficient knowledge of the dynamics of the vortex systems, and move on to the behavior of passive tracers generated by these flows.

IV. JETS

A. Definitions

As previously mentioned, the motion of point vortices is chaotic for both systems of 4 or 16 vortices, but the use of Poincaré maps in these cases is impossible, in contrast to [21,23,24]. To investigate the anomalous transport properties from the first principles, it is crucial to define a proper diagnostic that will be able to capture some singular properties of the dynamics that are clues to the origin of the anomalous transport of passive tracers.

For the system of 4-point vortices, successive snapshots have shown that passive tracers can stick to the boundaries of cores and jump from one core to another or escape from the core due to their perturbations. The fact that a tracer is able to escape from a core means that the surrounding regions of the cores are connected to the region of strong chaos. The results presented in [25] indicate that these regions mix poorly with the region of strong chaos. One way to track this phenomenon is to use finite-time Lyapunov exponents (FTLE) and to eliminate domains of small values of the FTLE [58,69,70]. Once these exponents are measured from the tracers' trajectories, whose initial conditions are covering the plane, a scalar field distributed within the space of initial conditions is obtained and the two-dimensional plot of the scalar field reveals regions of vanishing FTLE, namely, the cores surrounding the vortices and the far-field region. The cores are thus regions of small FTLE, meaning that two nearby trajectories are bound together for long times, despite the core's chaotic motion. These properties reveal typically a sharp change of the tracers dynamics as it crosses from the region of strong chaos to the core. This property is directly linked to the method described in [68], which determines from a Lagrangian perspective the border of coherent structures in a turbulent flow. Namely, the method consists in computing a scalar field (typically FTLE's) and extracting the coherent structures by finding the spatial extrema of this scalar field. The difficulty with these types of approach resides in the definition of the Lyapunov exponent,

$$\sigma_L = \lim_{\tau \to \infty} \lim_{r(0) \to 0} \frac{1}{\tau} \ln \frac{r(\tau)}{r_0}, \tag{22}$$

where r_0 is the initial separation between two nearby trajectories and $r(\tau)$ is the separation at time τ. Indeed, definition (22) introduces an arbitrary choice of two free parameters when computing FTLE, namely, the initial separation between two different trajectories r_0 and the time interval τ within which they are computed. Moreover, FTLEs are not unique for a given trajectory, which induces also a dependence on initial conditions x_0, as well as time if the system is not autonomous. In the following, we shall note FTLE as σ_L, but shall keep in mind that $\sigma_L = \sigma_L(\tau, r_0, x_0, t)$.

One problem that may arise while computing these exponents is related to the behavior of $r(t)$. For instance, in the case of a system of four identical point vortices, the motion of tracers is more or less confined within a finite-sized region and $r(t)$ has an upper boundary $R(t)$, which may be dependent on time if radial diffusion occurs, and no matter what initial distance r_0 and initial position x_0, $\sigma_L \to 0$ as $\tau \to \infty$. This example is rather extreme and exaggerated as the results presented in [58] are able to capture the structure of the space of initial conditions, but we believe it illustrates clearly one problem encountered when using FTLE, namely, that $r(t)$ is dependent on possible scales of the physical nature of the system. It is likely that $r(t)$ is not always a smooth growing function of the time on the scale of an arbitrary time τ and jumps between different spatial scales with a potential physical meaning, which may get averaged with the time. We can anticipate that this may be the case especially when different regions of small (if not zero) Lyapunov exponents are present in the system.

From the preceding discussion it appears that FTLEs are giving us overall good results in detecting coherent structures and regions of low chaos, but may also hide by averaging out useful information as a result of not capturing specific scales. In the following, we propose an alternative diagnostic, which is largely inspired by typical FTLE but has the advantage of eliminating some of its shortcomings. Namely, FTLE is a straightforward approximation of definition (22) of the Lyapunov exponent, which is inherently nonlocal. In other words, a Lyapunov exponent measures the ''averaged'' exponential divergence of two nearby trajectories and, assuming the system is ergodic, it measures a degree of ''chaoticity'' of the whole dynamics of the considered system. This nonlocality property may create serious difficulties in the interpretation of the results when the truncated characteristics of the dynamics have been used while for the considered time interval the ergodic theorem may not work (see more discussion in Ref. [59]).

One possible way to circumvent this problem can be identified by the following remarks. Most of the time we are dealing with only a finite portion of a trajectory (finite time) and only have a finite spatial resolution of these pieces of trajectories, which is typically much smaller than the actual scales we are interested in. In this more practical situation, we are facing a ''coarse grained'' phase space, and each point is actually a ball from which infinitely many real trajectories can depart. Given these facts, we can imagine that two nearby real trajectories diverge exponentially for a while but then get closer again without actually leaving the ball, a process which may take place over and over in the case of stickiness. From the ''coarse grained'' perspective those two real trajectories are identical. We can then infer that there exists a bunch of nearby trajectories that may remain within the ball for a given time, giving rise to what is called a *jet* [59], and can be understood as a region of regular motion for

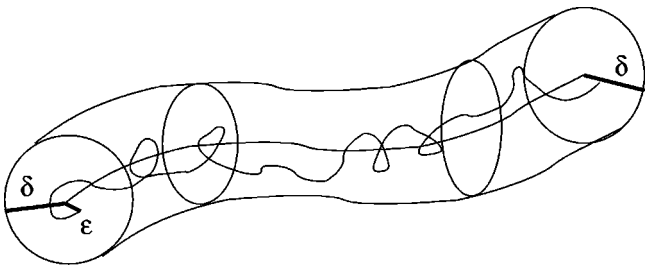

FIG. 5. A tracer and a ghost are used to define a jet.

our scale of interest (see Fig. 5). We are then mostly interested in the chaotic properties of the system from the ball scale and disregard any chaotic motion that may occur within the jet. The stickiness to a coherent structure that is randomly moving and not well determined in phase space implies the existence of jets, while the opposite may not be the case.

To actually measure the jet's system properties, we use the following strategy. Let us consider a given trajectory $\mathbf{r}(t)$ evolving within the phase space. For each instant t, we consider a ball $B(\mathbf{r}(t),\delta)$ of radius δ centered on our reference trajectory. We then start a number of trajectories within the ball at a given time and measure the time it actually takes them to escape the ball. Depending on how rapidly trajectories are escaping the ball, we should then be able to identify if the reference trajectory is moving within a regular jet or is in a region of strong chaos.

B. Statistical Results

From the numerical point of view, we first consider the velocity field generated by the chaotic motion of four-point vortices and proceed as follows: given an initial condition of a tracer, two particles are placed in its neighborhood, at a distance $\epsilon = 10^{-6}$. We refer to such a particle as a ''ghost'' to differentiate it from the referenced tracer. More specifically, we placed one ghost on the tracer speed and the other one on the orthogonal direction, but this positioning should not affect the results. Then for each of the ghost particles, once it reaches a distance $\delta = 0.03$ (the radius of our ball) from the tracer, the time interval Δt and the distance traveled Δs are recorded. For simplicity, two new ghost particles are placed within the ball once both have escaped, while the old ones are discarded. One of the main difficulties in using this type of diagnostic lies in the fact that data acquisition is *a priori* not linear in time or space and necessitates a careful choice for the values of ϵ and δ. Note that the value chosen for δ is small even compared to the minimum intervortex distance. However, using definition (22), we can compute a different type of FTLE, which we define as follows:

$$\sigma_L = \frac{1}{\Delta t}\ln\frac{\delta}{\epsilon}, \quad \sigma_D = \frac{1}{\Delta s}\ln\frac{\delta}{\epsilon}, \tag{23}$$

where, contrary to the typical definitions, the value of the logarithm is fixed and Δt or Δs are the variables. These exponents are very similar to the notion of finite-size Lyapunov exponent (FSLE) considered in [71]; however, we do not perform averages over different scales and keep the whole distribution function. We computed these exponents for the flow generated by four vortices with the same initial condition as the one used in [25]. The data are obtained using the trajectories of four different tracers initially placed in the region of strong chaos and advected by the chaotic flow generated by the motion of the four-point vortices of equal strength. The time of the simulation is 5×10^6, the time step is 0.05, which leads to statistics computed using $\sim 3.10^5$ data points. The results of the measured σ_L are illustrated in Fig. 6. In this plot, one can see two different types of behavior.

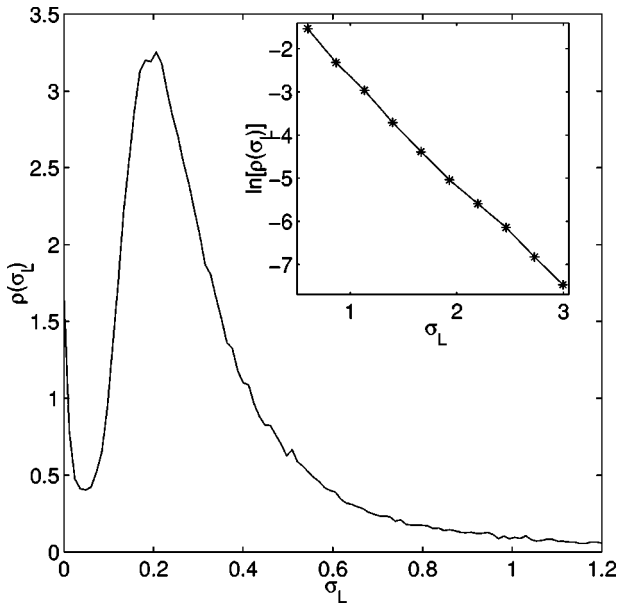

FIG. 6. Distribution of time Lyapunov exponents σ_L [see Eq. (23)]. We note an exponential decay for high exponents. $\rho(\sigma_L) \sim \exp(-\sigma_L/\sigma_{L_0})$ with $\sigma_{L_0} \approx 0.4$. We can see a minimum around $\sigma_L \approx 0.05$. The observed accumulation near 0 results from the existence of long-lived jets. The local minimum gives an estimate of the minimum typical time interval corresponding to a jet: $\Delta t_{min} \approx 206$. Data are obtained with four different trajectories computed up to $t = 5\times10^6$, leading to 328 220 records.

First, the large FTLE decay exponentially with a characteristic exponent $\sigma_{L_0} \approx 0.4$, which is not surprising, since the speed of the tracers is bounded. Hence even if the tracer and the ghost are going in opposite directions, it will always take them a finite time to escape from the ball, thus an expected maximum value for σ_L. Regarding the exponential decay behavior before reaching this maximum value, we can suspect it is directly related to the way the data is acquired; indeed, we remind the reader that the acquisition is *a priori* nonlinear in time, and that we are in fact measuring escape times from a given moving region of the phase space, and since this behavior is related to the large FTLE's, we are just observing the exponential growth of the coarse grained volume.

The second behavior is, from the point of view of anomalous transport, more interesting. The local minimum for small FTLE can be seen in the probability density of σ_L as a crossover from the erratic chaotic motion of the tracer within the chaotic region to its motion within a quasiregular jet. Indeed, if the tracer is within the jet, the ghosts are neverthe-

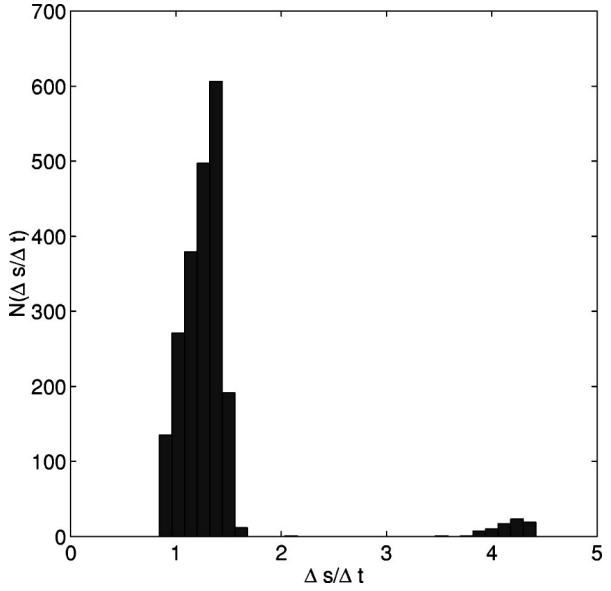

FIG. 7. Distribution of the averaged speed of the tracer for the data corresponding to $\sigma_D < 0.03$. We observe two regimes; the regime of fast speed corresponds to stickiness to the core. Note that if instead we use σ_L as a reference, most of the fast particles lie beyond the local minimum in the distribution and mostly only one regime seems to be present.

less expected to escape from the tracer's vicinity but with trapping times exhibiting a power-law decay; therefore, if the passive tracer is evolving within a jet for a long time, we should expect an accumulations of events corresponding to ghosts leaving the surrounding ball. This hypothesis is confirmed by analyzing the tail of the distribution of trapping times plotted. Using the data from Fig. 6, we measured a power-law decay, with some oscillations and whose typical exponent $\rho(t) \sim t^{-\gamma}$ gives $\gamma \approx 2.823$.

We shall now discuss the reason why another Lyapunov exponent σ_D was introduced in Eq. (23). By its definition σ_D measures how much the two trajectories diverge depending on how far along them we travel. It is then inherently time independent and can be seen as a pure geometric property of a trajectory or, from another point of view, time is locally rescaled depending on the local speed, so that the speed along the trajectory is constant and equal to one. The plot of the distribution of σ_D gives the same picture as the one obtained for σ_L in Fig. 6, with an exponential decay and a local minimum $\sigma_D^* \sim 0.03$ near zero, which also can be used as a criterion for identifying a coherent jet. We may argue that since the speed is bounded and almost nonzero everywhere, the use of σ_D is redundant and therefore futile. Nevertheless, from a practical point of view, the interval of possible speed is rather large; for instance, in the case of the four-vortex system, the core has a typical radius of 0.2 while the outer region corresponds to radii of around 4. We can thus expect an order of magnitude between the different speeds within the region of strong chaos and the outer region; moreover, we can expect an increase in the range as we increase the number of vortices. It then becomes obvious that by measuring σ_L we are biased towards jets occurring in the outer region, while by using σ_D these dynamical differences are erased and only the actual topology of the vicinity of a trajectory matters. Hence when using σ_D^* to characterize a jet in a small simulation, we obtained for the distribution of characteristic speeds the histogram plotted in Fig. 7, where it clearly shows that actual fast jets exist; had we used only σ_L, only a few fast jets would have been detected. In light of this, it seems that σ_{D*} is a good candidate for identifying a jet, while its averaged speed σ_L/σ_D gives a more refined idea of the nature of the jet.

C. Jets pictures

Given the preceding results, we shall now have a closer look at those jets. Namely, in the preceding sections we defined what we considered a jet, computed statistics on them, and using the results, we were able to obtain a threshold for which a jet can be considered regular. We then just have to apply these results. Let us initialize a tracer in the region of strong chaos, but not in the vicinity of any vortex to avoid any trapping within a core. We can let the tracer evolve with its two ghosts nearby, once the threshold given by σ_D^* is reached (ghosts are still within the ball for a given length traveled), we know that the measured σ_D will be such that $\sigma_D < \sigma_D^*$, hence we are currently within what we considered a regular jet. We then just have to record the position of the tracer and vortices until the ghosts have escaped. In this way we are able to locate the tracer for a given length of time while it evolves within the jet. In fact, we shall be even more choosey, namely, we know from Fig. 7, that the majority of jets correspond to slow motion, which when plotted correspond to the tracer being in the far-field region and simply rotating around the center of vorticity. Hence to avoid recording the position of these events, we can also use the averaged speed σ_L/σ_D and record only the jets corresponding to fast motion.

The analysis of a portion of a detected single fast jet is illustrated in Fig. 8. This jet corresponds to a trapping time of the ghosts $\Delta t \approx 560$. Since we suspected that a jet would be located within the sticky zones surrounding the vortex cores, we verified that the tracer is always in the vicinity of a vortex during the jet; moreover, we also note that during its evolution, the tracer jumps from one vortex to another. The full jet resumes as follows: first the tracer is close to vortex 1, then it jumps to vortex 3, then to vortex 4, then back to vortex 3. This result is consistent with the observations made in [25] that the sticky zone is where all surrounding vortices reunite. The possibility of the formation of a pair of two bound vortices as well as the role of these pairings allowing tracers to jump between vortices as well as trapping (freeing) them within (from) sticking zones described in [25] lead us to assume that pairing was the cause of the odd behavior of the tracer. This is confirmed in Fig. 8(d), where the distance between the two concerned vortices is plotted and a pairing of the two vortices is observed for the time interval $150 < t < 200$.

The actual history of the jets is plotted in two different reference frames in Fig. 8. Note that the absolute position of the tracer as it evolves in the jet looks random, hence we plotted in Fig. 8(b) the position of the tracer in the reference

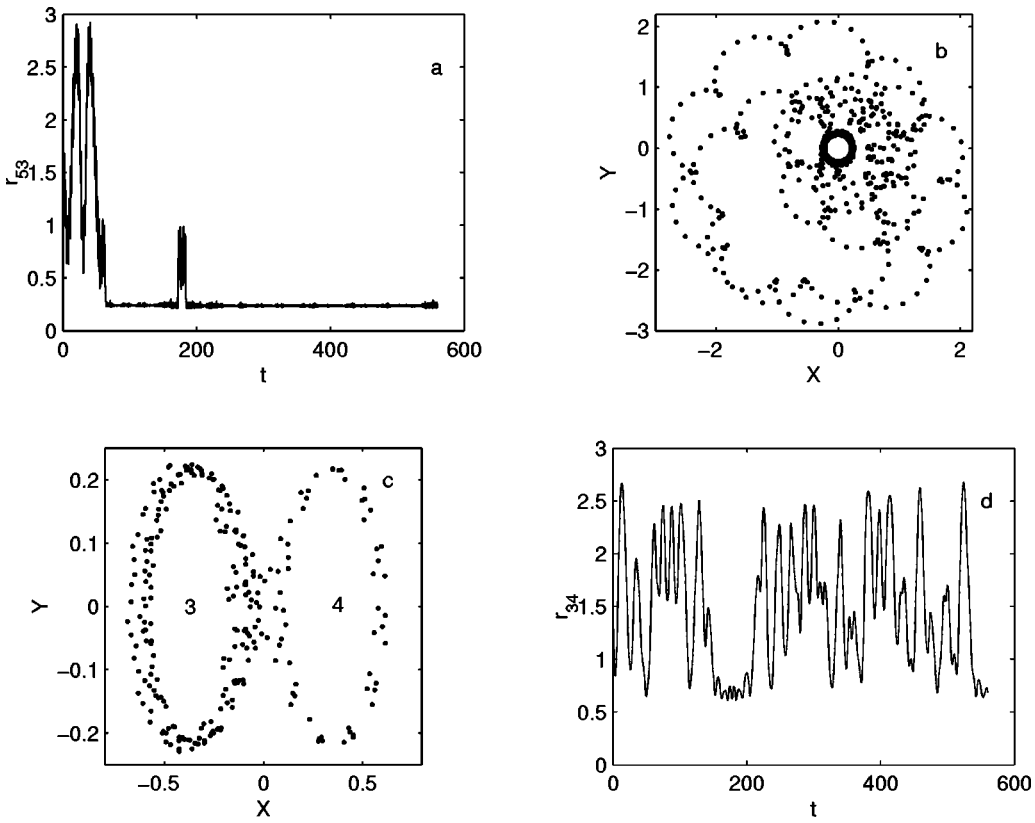

FIG. 8. Plots of tracer's positions and relative distances for different times for an identified jet within the ''strong chaos'' area for which $\Delta t \approx 560$. Plot (a) shows the distance between the passive tracer and vortex 3 vs time (the tracer is referred to as particle 5). Plot (b) shows the relative position of the tracer with respect to vortex 3; we observe the sticking habits of the tracer. Plot (c) shows the relative position of the tracer with respect to the pair formed by vortices 3 and 4 during the pairing ($153 < t < 205$). Plot (d) shows the distance between vortices 3 and 4 vs time. We note that for this jet the passive tracer sticks to vortex cores. It can jump from core to core as vortices are pairing but is always sticking to one core.

frame which is moving with vortex 3 [the one with whom the tracers spend most of their time as seen in Fig. 8(a)], and the sticking behavior of the tracer during the jets becomes clearer. In Fig. 8(c), we plotted the position of the tracer during the pairing of vortices 3 and 4 observed in Fig. 8(d) in the reference frame whose origin is the center of vorticity of the pair and which rotates such that the vortices are stuck oscillating in the x direction. The double jump from one vortex back and forth and the exchange between cores is illustrated.

This visualization of the location of the jets has confirmed the results already illustrated in [25]—that the boundaries of the core exhibit the stickiness. However, we would like to emphasize the fact that in the present case, this property of the system has been diagnosed with the use of coherent jets, in other words, by analyzing the relative evolution of two nearby trajectories within a specific scale (phase space ball). In this sense the method used is rather general, while in [25] a more detailed knowledge of the system was necessary to capture its ''hidden order.'' To test the method even further, we decided to apply it to the system of 16 vortices considered in Sec. III. Given the previously obtained threshold for four vortices, we skipped the analysis of the distributions of σ_L, σ_D and used the similar values to attempt the detection of a fast jet in the flow generated by 16 vortices. A jet is effectively detected and is illustrated in Fig. 9, meaning that the method is relatively robust since in this 16-vortex system the cores are much smaller. In this last figure the fluctuations of r_2 increase towards the end because a pairing occurs between vortex 2 and another one; both ghosts have escaped but they may have jumped onto the other core while the tracer is still sticking, or vice versa. Besides this, we also get from Fig. 9 the actual size of the core, which is typically $r \sim 0.044$ and is within a reasonable range of the estimate given by the half of the minimum distance reached between vortices $\min(r_{ij})/2 \sim 0.06$, a fact which was also observed for 3- and 4-vortex systems [24,25].

In the following section we will explore a little further the notion of the jets as coherent structures.

D. Jet structure analysis

In the preceding section we were able to establish that a given tracer was evolving within what we called a jet once a given threshold σ_D^* for the measured σ_D was reached, and were then able to visualize the jet by recording the tracer's position. In the meantime, we could also record the positions of the ghosts. We should be then able to gather some information about the inner structure of the jet. This should incur very little numerical overload other than perhaps the need for more storage space.

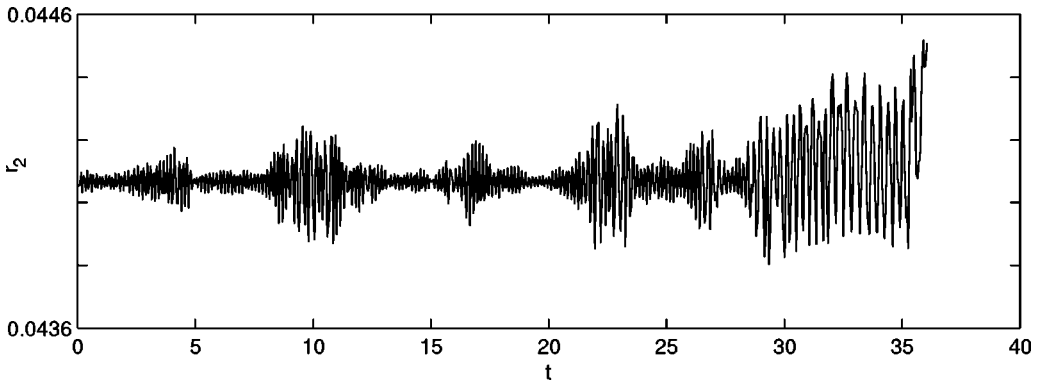

FIG. 9. Distance between the tracer and vortices for coherent jets detected in the system of 16 vortices. The distance relative to vortex 2 is plotted.

In order to take advantage of this possibility, we looked for a longer lived jet, which, for the four-vortex case, was easier to find in the far-field region. Plots of such a long-lived jet are presented in Fig. 10, where we can see a fine structure within the jet, which seems to be formed of a hierarchy of circular (tubular) jets within jets. Wondering if these features were general or specific to these four-vortex systems, we decided to consider the fast jet illustrated in Fig. 9 and check its structure. The results are plotted in Fig. 11, where the relative position of the ghost is plotted with different shades of grain corresponding to different time periods of the life of the jets. We can see that effectively the nested set of jets within jets remains, and that the ghost is also spiraling back and forth in between. This figure is also informative in the sense that we actually see the ghost going back very close to the tracer. In other words, the area characterized by the gray points close to the origin in Fig. 11 does not correspond to the beginning of the jet and, therefore, is not an artifact of having initially placed the ghost in the vicinity of the tracer.

We shall close this section with a final remark on this ''matroshka'' structure of the jets. Namely, this nested structure suggests that for each identified jet we can define a suite (r_n), such that r_n is a decreasing function of n with $r_n \to 0$ and $n \to \infty$ and r_0 is, for instance, determined by the largest tube (jet) seen in Fig. 10 or Fig. 11. To each subjet n we can assign a distribution of trapping time $\rho_n(\tau)$ as well as a transit time t_n (or a distribution) associated with the tracer spiraling from one subjet n to one of its two neighbors $n-1$ or $n+1$. In light of this, depending on the transport properties, the whole system is likely to depend on the distributions $\rho_n(\tau)$ and the ratio r_n/r_{n+1}, and if we have in the limit $n \to \infty$ both $r_n/r_{n+1} \to r_\infty$ and $\rho_n(\tau) \to \rho_\infty(\tau)$, the FSLE become effectively independent of scale within the jet. This hierarchical structure is also reminiscent of the discrete renormalization group and hence we can speculate that the log-periodic oscillation described in [72] may be observed.

V. TRANSPORT PROPERTIES

A. Definitions

For the considered case, all vortices have positive strength and, therefore, are moving within a finite domain. It is important to define what quantities will be measured to characterize the transport properties of the system. There has been evidence in [58] of radial diffusion, but the diffusion coefficient D vanishes as $R \to \infty$ with typical behavior $D \sim 1/R^6$. In the case of more than four vortices, we can still expect a similar type of behavior. However, the far-field region is of little interest when one want to address the transport properties of typical geophysical flows, since the most relevant is the region being accessible to the vortices, i.e., the region of ''strong chaos.'' In fact, the same problem was faced when considering systems of three-point vortices. For these particular systems, the vortex motion is integrable, which restricts the accessible domain of tracers to within a finite region surrounded by a Kol'mogorov-Arnol'd-Moser curve. The way around this problem was then to measure how many times a tracer rotates around the origin, in other words, to measure the diffusion along an angular direction. However, even though suitable, this solution may face some criticism due to the singularity present at the origin. In this paper we consider tracer transport in the way already used with some success in [24]. Namely, we use the arclength $s(t)$ of the path traveled by an individual tracer up to a time t, which is

$$s_i(t) = \int_0^t v_i(t')dt', \tag{24}$$

where $v_i(t')$ is the absolute speed of the particle i at time t'. One advantage of this quantity is that it is independent of the coordinate system and as such we can expect to infer intrinsic properties of the dynamics. The main observable characteristics will be moments of the distance $s(t)$ defined in Eq. (24):

$$M_q = \langle |s_i(t) - \langle s_i(t) \rangle|^q \rangle, \tag{25}$$

where i corresponds to either the ith vortex or a tracer in the field of 4 or 16 vortices. The averaging operator $\langle \cdots \rangle$ needs a special comment. Expecting anomalous transport, one should be ready to have infinite moments starting from $q \geqslant q_0$. Specifically, it can be $q_0 = 2$. The value of q will vary from 0 to 8. To avoid any difficulty with infinite moments, we consider truncated distribution function

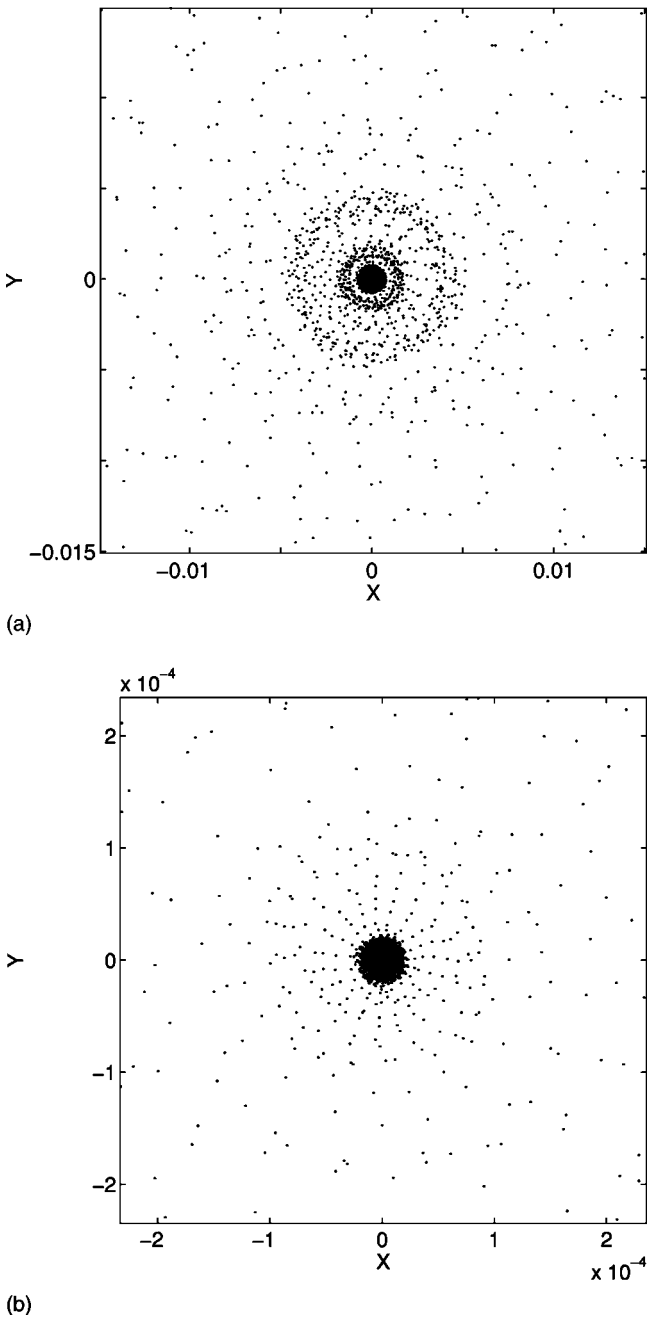

FIG. 10. Relative evolution of a ghost within a long-lived jet located in the far field region of the flow generated by four vortices. (a) is a centered zoom of (b) (see the scales). The distribution within the jet is clearly not uniform, suggesting a possible order organized as ''matroshkas'' (a nested set of jets with increasing radii).

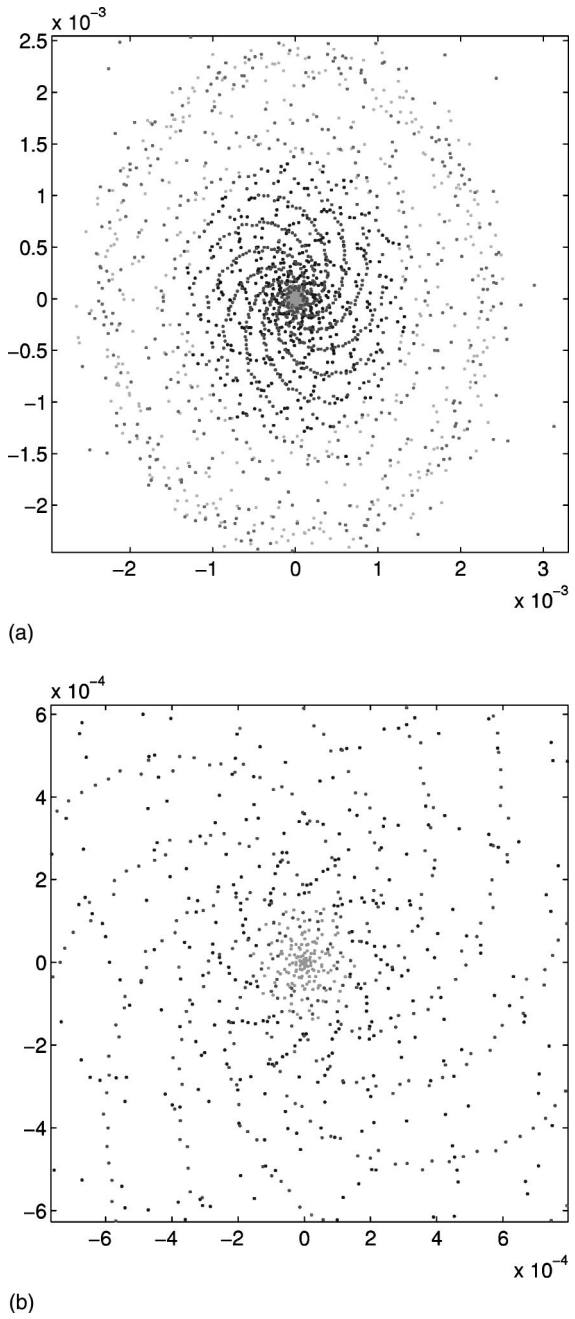

FIG. 11. Jet structure for a long-lived jet located in the region of strong chaos for a system of 16 vortices. (b) is a zoom of (a) corresponding to a magnification of an order of magnitude. The different shades characterize different moments of the life of the jet corresponding to approximately equal time intervals. They chronogically range as light, dark, and light. We see a similar structure of jets within a jet as observed in Fig. 10, and ghosts spiraling back and forth between them.

$$\rho_{tr}(s_i)=0, \quad s_i>s_i^*. \tag{26}$$

Condition (26) was discussed in detail in [73] to satisfy the physical restriction of a finite velocity. This condition put some constraints on the maximum value q^* of q corresponding to the maximum time t^*, beyond which the moments are basically monitoring the population of almost ballistic trajectories.

Up to the contraints mentioned, we will always consider the operation of averaging to be performed over truncated distributions. In this perspective all moments are finite and one can expect

$$M_q=\langle|s_i(t)-\langle s_i(t)\rangle|^q\rangle\sim D_q t^{\mu(q)} \tag{27}$$

with, generally, $\mu(q)\neq q/2$ as one would expect from normal diffusion. The nonlinear dependence of $\mu(q)$ means multi-

fractality of the transport. Some authors use the notion of weak $[\mu(q)=\text{const}\times q]$ and strong $[\mu(q)\neq\text{const}\times q]$ anomalous diffusion [69,70] or strong and weak self-similarity [74]. For more information on the appearance of multifractal kinetics and related transport, see [75,76].

B. Vortex transport properties in 16 vortex system

Due to the low dimensionality of a system of four-point vortices, no typical transport behavior has been measured, but there is an analysis of the phase space topology and Poincaré sections [25]. The results for 16 vortices were computed by using a number of different ''equivalent'' initial conditions. Such different trajectories were obtained by letting a given initial condition evolve and recording the positions of the vortices at different times with a given accuracy (typically 10^{-5}), while making sure no vortices were initially involved in pairings. The strong chaoticity of the system leads very rapidly to different trajectories while this choice of initial conditions lets us keep the constant of motions within a relatively small error. The transport properties are then obtained by averaging over all vortices as well as over different sets of trajectories that correspond to our specific arbitrary choice of the constants of motion. The results are presented in Fig. 14, where the exponent characterizing the long time power-law behavior of different moments is plotted versus moment order. The actual value of the second moment, which is typically used to characterize the transport properties, is measured to be $\mu(2)\approx 1.80$ and indicates a strong superdiffusive behavior of the vortex subsystem. This behavior can be linked to the pairing of vortices, which induces a strong quasiballistic dynamics of both vortices of the pair. Indeed, let us compare the exponent $\gamma\approx 2.68$ characterizing the distribution of time from which vortices are trapped into a pair measured in Fig. 4, and the value corresponding to the second moment behavior from Fig. 13. We see good agreement with the expected law $\gamma\approx\mu(2)+1$ [23,67]. From this observation we can conclude that the superdiffusive behavior of a vortex from the system of 16 vortices is related to the pairing phenomenon. Now we shall investigate the properties of tracers and we start with the chaotic flow generated by four vortices.

C. Passive tracers in a 4-vortex system

The results describing the transport properties of passive tracers are illustrated in Fig. 12. We also observe strong anomalous behavior for the tracers with an exponent for the second moment $\mu(2)\approx 1.82$. This behavior was previously observed in [23] for integrable flows driven by three vortices. In this latter case, the origin of the anomalous behavior was directly linked to the presence of islands of regular motion within the stochastic sea and the phenomenon of stickiness observed around them. In the present case the driving flow is chaotic but nevertheless the existence of cores surrounding the vortices and the far-field region allows a direct analogy and we may say that the tracer meets similar structures. The only difference is that some of the structure elements (the cores) are ''mobile.'' Moreover, the previous study [23,25] shows that tracers effectively stick to the vortex cores, and the FTLE field presented in [58] shows that in the far-field region the motion of tracers is quasiballistic, which is a good indication of sticking behavior.

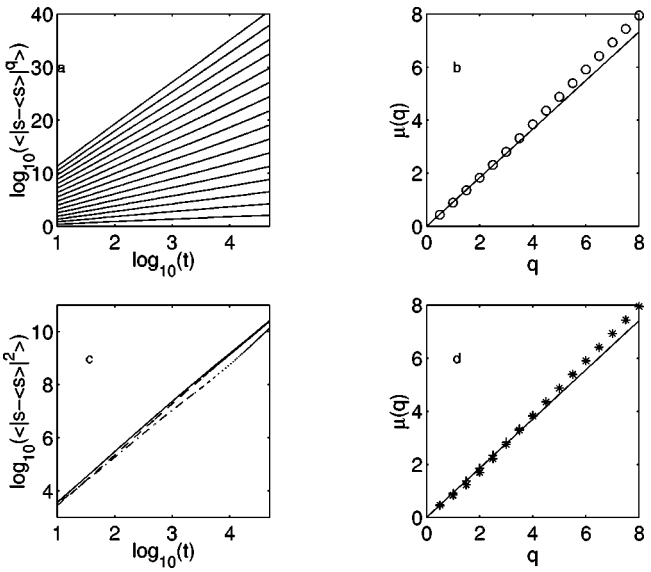

FIG. 12. Plot of different transport properties of tracers in a 4-vortex system. (a) the different moments vs time are plotted for $q=1/2,1,\ldots,8$. (b) Long time exponent behavior for the different moments [see Eq. (25)], with $\mu(2)\approx 1.83$ corresponding to a superdiffusive regime. (c) Second moment vs time; the full line corresponds to the full data, the dashed line is computed with all trajectories except the parts sticking to vortices, and the dot-dashed line corresponds to all trajectories except the part sticking to the outer region. (d) Different exponents for partial data; *, outer region cut ($\mu_f=1.7$); +, vortex-sticking cut ($\mu_s=1.85$); in both cases the transport is anomalous and superdiffusive.

This conclusion can be strengthened by considering previously described jets. We have seen that the jets are located in the sticky regions, and are either moving around cores and jumping from core to core or rotating in the far-field region. Since we now have ''mobile'' sticky regions traced by the long-lived jets, which we are able to monitor, we can estimate that the sticking time (or trapping time in the sticky zone) is more-or-less similar to the time it takes for a ghost to escape a long-lived jet, hence the power-law behavior of the tail of the trapping time distribution characterize the exponent γ. We then actually observe an exceptional agreement with the expected $\gamma\approx\mu(2)+1$ relation. Hence since the notion of jet as defined in Sec. IV is relatively general when compared to the notion of core or far-field region, we shall say that the anomalous diffusion finds its origin in the existence of long-lived ''coherent'' jets of passive tracers for the chaotic flow generated by four vortices. Since we know that two different types of jets exist (see Fig. 7) and are able to differentiate them easily, in a similar manner as for the 3-vortex case [23,24] we are able to quantify the influence of each type of jet on the transport properties of the system by discarding tracers evolving within a given type of jets. The results of this analysis are presented in Fig. 12, plots (c) and (d). We can conclude that both types of jets give

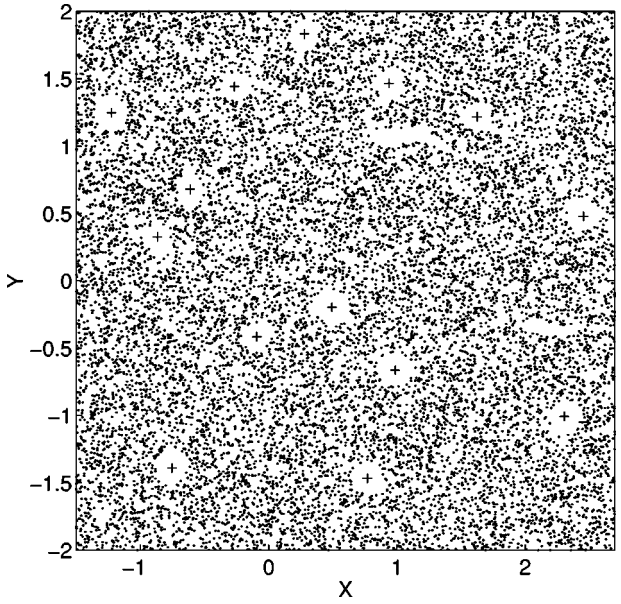

FIG. 13. Local snapshot of the system of 16 vortices with 9×10^4 tracers. The vortices are located with the "+" sign. We can see the cores surrounding the vortices. The snapshot is taken early in the simulation to prevent too much dispersion of the tracers and to visualize the core. As a consequence, we can expect the actual sizes of the cores to be a little smaller than the radius of $r\approx0.1$ that one can measure on the snapshot.

rise to anomalous transport with very similar characteristic exponents and that they both contribute to the observed strong anomalous diffusion.

D. Passive tracers in a 16-vortex system

In both previous cases we observed a signature of anomalous superdiffusion with $\mu(2)\approx1.8$. Let us now investigate the transport properties of passive tracers in a flow generated by 16 identical point vortices, described partially in Sec. III. There are long-lived jets within the region of strong chaos (see Fig. 11) for the flow and the detected jet lives in the vicinity of a vortex and probably sticks to its core. A snapshot of the system at an early stage is given in Fig. 13, which effectively identifies the cores surrounding the vortices. The results describing the transport properties of passive tracers are presented in Fig. 14 and show strong anomalous behavior with the exponent $\mu(2)=1.77$.

Even though we only consider one arbitrary initial condition of the vortex system, it is reasonable to assume that the transport properties obtained for such a system are fairly general in the sense that they persist with an increase in the number of vortices if the probability of pairing persists. That implies the possibility of neglecting the occurrence of more complicated long-lived clustering, such as the triplet observed in Fig. 2, quadruples, etc.

VI. CONCLUSION AND DISCUSSIONS

In this paper we have investigated the dynamical and statistical properties of the vortex and passive particle advection in chaotic flows generated by 4- and 16-point vortices. The

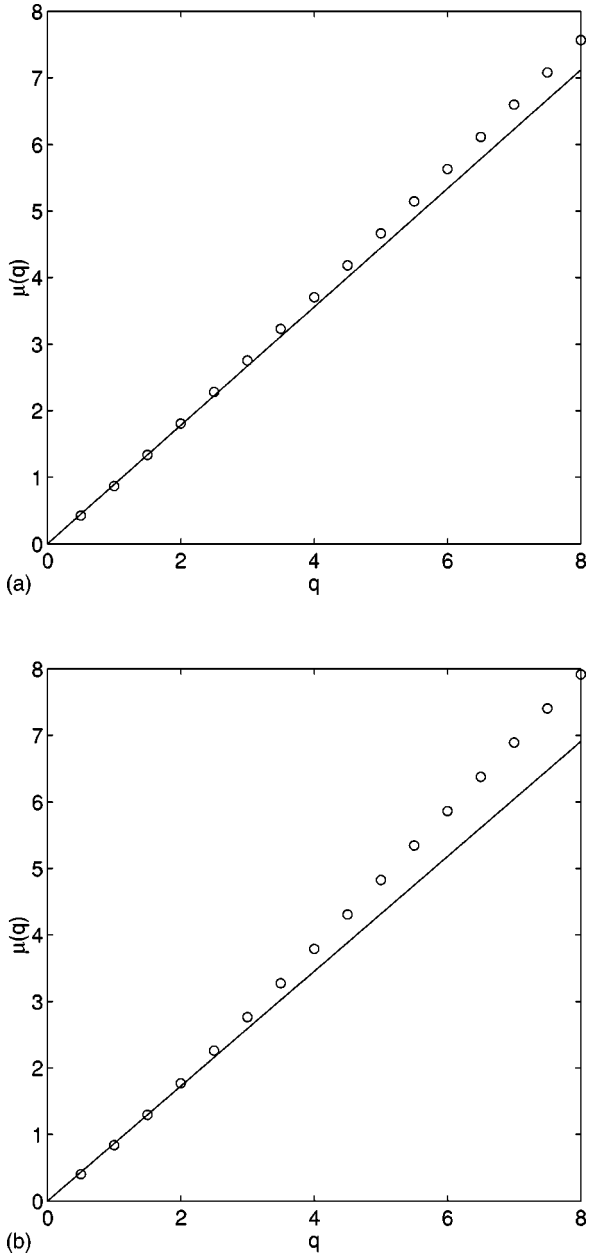

FIG. 14. Large-time behavior for the different moments $\langle|s(t)-\langle s(t)\rangle|^q\rangle\sim t^{\mu(q)}$. In (a) the flow of 16-point vortices, with $\mu(2)\approx1.80$ while in (b) the tracer moments for the flow driven by the 16-point vortices, with $\mu(2)\approx1.77$ (the slope for small q is 1.75 and for large q is 1.95).

goal of this work was to provide qualitative insight into general transport properties of two-dimensional flows, especially geophysical ones, imposed by the topology of the phase space. The system of 16 vortices can be considered as a fairly large system while the 4-vortex system is the minimal one with chaotic dynamics of the vortices. The time-averaged spatial distribution of the vortices is characterized by a nonuniform density of vorticity, which implies strong vortex-vortex correlation. These correlations manifest themselves by way of a phenomenon of stickiness, namely, the formation of long-lived pairs of vortices, triplets, etc. Since both these structures are integrable, we can speculate that the

stickiness occurs by forming quasi-integrable subsets. The clusters of vortices can form a hierarchical or nested set of integrable subsets and hence impose some constraints on the frame of possible larger structures involving more vortices. The statistics of pairing time exhibits a power-law tail confirming in that way the sticky nature of the phenomenon, which in return allows us to make an analogy with an ideal dynamical system and give a good analytical estimate of the characteristic exponent of the pairing time distribution.

The chaotic nature of the governing flows did not allow the use of diagnostics, such as Poincaré maps or distribution of recurrences, commonly used for systems with 1-1/2 degrees of freedom, hence a technique inspired by finite-time Lyapunov exponents diagnostics has been put into place. Passive tracer motion is analyzed by measuring the mutual relative evolution of two nearby tracers. The possibility of tracers traveling in each other's vicinity for relatively large times confirmed the presence of a hidden order for the tracers, which we call jets. The jets can be understood as moving clusters of particles within a specific domain where the motion is almost regular from a coarse-grained perspective. The chaotic nature of the motion is confined within the characteristic scale of a given jet, where nearby tracers are trapped. The distribution of trapping times in the jets shows a power-law tail whose characteristic exponent is quantitatively very similar to the one related to pairing times. The calculated Lyapunov exponent for tracers within the jet's exponents are similar to what is called finite-sized Lyapunov exponent [74], but in our calculations no average is taken and thus a distribution is obtained. These distributions of the Lyapunov exponents exhibit a finite local minimum, which results from the competition of the trapping in jets and the strongly chaotic motion outside the jets. The existence of this minimum allows a dynamical test, which identifies whether a tracer is trapped within a jet and thus allows one to localize the jet in phase space. Jets are found to exist on the boundary of the cores surrounding the vortices as well as on the outer rim, the region to which vortices have no access. This behavior is analogous to the sticking behavior observed in the three-vortex case, and thus can be incorporated into the general notion of the phenomenon of stickiness. The differentiation between the two possible types of jets is determined entirely by the ratio of the corresponding pair of Lyapunov exponents. We thus obtain a *de facto* diagnostic to locate coherent structures. The method is then successfully applied to the system of 16 vortices, leading to a possible general dynamical mechanism of detecting coherent structures. Further analysis of the structure of the jets itself reveals a complicated nested structure of jets within jets, which indicates that jets exist at different scales. The distribution of trapping times within jets is computed and shows a power-law tail whose characteristic exponent is similar to the one observed for vortex pairing time. Since the trapping in jets is also a stickiness phenomenon, we may assume that the analytical estimate given for the vortex pairing time is also valid for the trapping time within jets. The transport properties of the 16 vortices as well as those of the tracers in both systems of 4 and 16 vortices are found to be anomalous with characteristic exponent $\mu \sim 1.75-1.8$. We would like to mention that the similarities found between the exponents for the tracers and the vortices in the 16-vortex system render plausible a causality relationship between the pairing of vortices and tracers being trapped within regular jets. All these results are in good agreement with the characteristic exponents of trapping times and the kinetic theory presented in Refs. [23,24]. Moreover, the transport properties are all of the multifractal type or strongly anomalous in the sense defined in Refs. [69,70]. This property of the transport is a consequence of the existence of different sticky zones and the related structures in phase space.

ACKNOWLEDGMENTS

The authors would like to thank L. Kuznetsov for very useful discussions. This work was supported by the U.S. Navy through Grant Nos. N00014-96-1-0055 and N00014-97-1-0426, and the U.S. Department of Energy through Grant No. DE-FG02-92ER54184.

[1] E. W. Montroll and M. F. Schlesinger, in *Studies in Statistical Mechanics*, edited by J. Lebowitz and E. W. Montroll (North-Holland, Amsterdam, 1984), Vol. 11, p. 1.
[2] J. P. Bouchaud and A. Georges, Phys. Rep. **95**, 127 (1990).
[3] *Levy Flights and Related Topics in Physics*, edited by M. F. Shlesinger, G. M. Zaslavsky, and U. Frisch (Springer, Heidelberg, 1995).
[4] M. F. Schlesinger, G. M. Zaslavasky, and J. Klafter, Nature (London) **363**, 31 (1993).
[5] G. Zimbardo, P. Veltri, and P. Pommois, Phys. Rev. E **61**, 1940 (2000).
[6] G. Złmbardo, A. Greco, and P. Veltri, Phys. Plasmas **7**, 1071 (2000).
[7] G. Manfredi, C. M. Roach, and R. O. Dendy, Plasma Phys. Controlled Fusion **43**, 825 (2001).
[8] S. V. Annibaldi, G. Manfredi, R. O. Dendy, and L. O'C Drury, Plasma Phys. Controlled Fusion **42**, L13 (2000).
[9] A. A. Chernikov, B. A. Petrovichev, A. V. Rogal'sky, R. Z. Sagdeev, and G. M. Zaslavsky, Phys. Lett. A **144**, 127 (1990).
[10] T. H. Solomon, E. R. Weeks, and H. L. Swinney, Physica D **76**, 70 (1994).
[11] E. R. Weeks, J. S. Urbach, and H. L. Swinney, Physica D **97**, 219 (1996).
[12] G. M. Zaslavsky, D. Stevens, and H. Weitzner, Phys. Rev. E **48**, 1683 (1993).
[13] S. Kovalyov, Chaos **10**, 153 (2000).
[14] A. Provenzale, Annu. Rev. Fluid Mech. **31**, 55 (1999).
[15] A. J. Majda and J. P. Kramer, Phys. Rep. **314**, 238 (1999).
[16] J. B. Weiss, A. Provenzale, and J. C. McWilliams, Phys. Fluids **10**, 1929 (1998).
[17] P. Tabeling, A. E. Hansen, and J. Paret, in *Chaos, Kinetics and Nonlinear Dynamics in Fluids and Plasma*, edited by S. Ben-

kadda and G. Zaslavsky (Springer, New York, 1998), p. 145.
[18] A. E. Hansen, D. Marteau, and P. Tabeling, Phys. Rev. E **58**, 7261 (1998).
[19] P. Tabeling, S. Burkhart, O. Cardoso, and H. Willaime, Phys. Rev. Lett. **67**, 3772 (1991).
[20] V. V. Meleshko and M. Yu. Konstantinov, *Vortex Dynamics and Chaotic Phenomena* (World Scientific, Singapore, 1999).
[21] L. Kuznetsov and G. M. Zaslavsky, Phys. Rev. E **58**, 7330 (1998).
[22] Z. Neufeld and T. Tél, J. Phys. A **30**, 2263 (1997).
[23] L. Kuznetsov and G. M. Zaslavsky, Phys. Rev. E **61**, 3777 (2000).
[24] X. Leoncini, L. Kuznetsov, and G. M. Zaslavsky, Phys. Rev. E **63**, 036224 (2000).
[25] A. Laforgia, X. Leoncini, L. Kuznetsov, and G. M. Zaslavsky, Eur. Phys. J. B **20**, 427 (2001).
[26] H. Aref, J. Fluid Mech. **143**, 1 (1984).
[27] G. M. Zaslavsky, R. Z. Sagdeev, and A. A. Chernikov, Zh. Éksp. Teor. Fiz. **94**, 102 (1988) [Sov. Phys. JETP **67**, 270 (1988)].
[28] J. Ottino, *The Kinematics of Mixing: Stretching, Chaos, and Transport* (Cambridge University Press, Cambridge, 1989).
[29] H. Aref, Philos. Trans. R. Soc. London, Ser. A **A333**, 273 (1990).
[30] J. Ottino, Annu. Rev. Fluid Mech. **22**, 207 (1990).
[31] V. Rom-Kedar, A. Leonard, and S. Wiggins, J. Fluid Mech. **214**, 347 (1990).
[32] G. M. Zaslavsky, R. Z. Sagdeev, D. A. Usikov, and A. A. Chernikov, *Weak Chaos and Quasiregular Patterns* (Cambridge University Press, Cambridge, 1991).
[33] A. Crisanti, M. Falcioni, and G. Paladin, and A. Vulpiani, Riv. Nuovo Cimento **14**, 1 (1991).
[34] A. Crisanti, M. Falcioni, A. Provenzale, P. Tanga, and A. Vulpiani, Phys. Fluids A **4**, 1805 (1992).
[35] R. Benzi, G. Paladin, S. Patarnello, P. Santangelo, and A. Vulpiani, J. Phys. A **19**, 3771 (1986).
[36] R. Benzi, S. Patarnello, and P. Santangelo, J. Phys. A **21**, 1221 (1988).
[37] J. B. Weiss and J. C. McWilliams, Phys. Fluids A **5**, 608 (1992).
[38] J. C. McWilliams, J. Fluid Mech. **146**, 21 (1984).
[39] J. C. McWilliams, J. Fluid Mech. **219**, 361 (1990).
[40] D. Elhmaïdi, A. Provenzale, and A. Babiano, J. Fluid Mech. **257**, 533 (1993).
[41] G. F. Carnevale, J. C. McWilliams, Y. Pomeau, J. B. Weiss, and W. R. Young, Phys. Rev. Lett. **66**, 2735 (1991).
[42] N. J. Zabusky and J. C. McWilliams, Phys. Fluids **25**, 2175 (1982).
[43] P. W. C. Vobseek, J. H. G. M. van Geffen, V. V. Meleshko, and G. J. F. van Heijst, Phys. Fluids **9**, 3315 (1997).
[44] O. U. Velasco Fuentes, G. J. F. van Heijst, and N. P. M. van Lipzig, J. Fluid Mech. **307**, 11 (1996).
[45] R. Benzi, M. Colella, M. Briscolini, and P. Santangelo, Phys. Fluids A **4**, 1036 (1992).
[46] J. B. Weiss, CRM Proc. Lecture Notes **20**, 109 (1999).
[47] O. Agullo and A. D. Verga, Phys. Rev. E **63**, 056 304 (2001).
[48] H. Aref, Phys. Fluids **22**, 393 (1979).
[49] H. Aref, Annu. Rev. Fluid Mech. **15**, 345 (1983).
[50] E. A. Novikov, Sov. Phys. JETP **41**, 937 (1975).
[51] J. L. Synge, Can. J. Math. **1**, 257 (1949).
[52] X. Leoncini, L. Kuznetsov, and G. M. Zaslavsky, Phys. Fluids **12**, 1911 (2000).
[53] J. Tavantzis and L. Ting, Phys. Fluids **31**, 1392 (1988).
[54] E. A. Novikov and Yu. B. Sedov, Sov. Phys. JETP **48**, 440 (1978).
[55] H. Aref and N. Pomphrey, Proc. R. Soc. London, Ser. A **380**, 359 (1982).
[56] S. L. Ziglin, Sov. Math. Dokl. **21**, 296 (1980).
[57] A. Babiano, G. Boffetta, A. Provenzale, and A. Vulpiani, Phys. Fluids **6**, 2465 (1994).
[58] S. Boatto and R. T. Pierrehumbert, J. Fluid Mech. **394**, 137 (1999).
[59] V. V. Afanasiev, R. Z. Sagdeev, and G. M. Zaslavsky, Chaos **1**, 143 (1991).
[60] H. Lamb, *Hydrodynamics*, 6th ed. (Dover, New York, 1945).
[61] R. I. McLachlan and P. Atela, Nonlinearity **5**, 541 (1992).
[62] E. Ott, *Dynamic Chaos* (Cambridge University Press, Cambridge, 1998).
[63] V. K. Melnikov, in *Transport, Chaos and Plasma Physics II*, edited by F. Doveil, S. Benkadda, and Y. Elskens (World Scientific, Singapore, 1996), pp. 142–153.
[64] V. Rom-Kedar and G. M. Zaslavsky, Chaos **9**, 697 (1999).
[65] V. V. Meleshko and M. Yu. Konstantinov, *Vortex Dynamics and Chaotic Phenomena* (World Scientific, Singapore, 1999), Vol. 7, p. 159.
[66] G. M. Zaslavsky, M. Edelman, and B. A. Niyazov, Chaos **7**, 159 (1997).
[67] G. M. Zaslavsky and M. Edelman, Chaos **10**, 135 (2000).
[68] G. Haller and G. Yuan (unpublished).
[69] P. Castiglione, A. Mazzino, P. Mutatore-Ginanneschi, and A. Vulpiani, Physica D **134**, 75 (1999).
[70] K. H. Andersen, P. Castiglione, A. Mazzino, and A. Vulpiani, Eur. Phys. J. B **18**, 447 (2000).
[71] E. Aurell, G. Boffetta, A. Crisanti, G. Paladin, and A. Vulpiani, J. Phys. A **30**, 1 (1997).
[72] S. Benkadda, S. Kassibrakis, R. White, and G. M. Zaslavsky, Phys. Rev. E **59**, 3761 (1999).
[73] H. Weitzner and G. M. Zaslavsky, Chaos **11**, 384 (2001).
[74] R. Ferrari, A. J. Manfroi, and W. R. Young, Physica D **154**, 111 (2001).
[75] G. M. Zaslavsky, Physica A **288**, 431 (2000).
[76] G. M. Zaslavsky, in *Application of Fractional Calculus in Physics*, edited by R. Hilfer (World Scientific, Singapore, 2000), p. 203.